Journal of Membrane Science 618 (2021) 118712

Contents lists available at ScienceDirect

Journal of Membrane Science

journal homepage: http://www.elsevier.com/locate/memsci

Selective protein purification via tangential flow filtration – Exploiting protein-protein complexes to enable size-based separations

Ivan S. Pires, Andre F. Palmer *

William G. Lowrie Department of Chemical and Biomolecular Engineering, The Ohio State University, 151 West Woodruff Ave, Columbus, OH, 43210, USA

ARTICLE INFO

Keywords:
Tangential flow filtration
Purification
Protein
Model
Protein-protein complex

ABSTRACT

Tangential flow filtration (TFF) is a size-based separation method conventionally used for buffer exchange, concentration, pathogen removal, and for coarse purification. In this study, we use TFF for selective purification of proteins in their complexed form. This process was demonstrated to recover human serum albumin (HSA) in its complexed form from an artificially produced mixture of hemoglobin (Hb) and HSA and from plasma using an anti-HSA polyclonal immunoglobulin G (IgG) as the target-protein binding molecule (TPBM). Moreover, haptoglobin (Hp) in its complexed form was recovered from human Cohn Fraction IV using Hb as the TPBM. Hb-Hp was then partially dissociated with 5 M urea to yield Hp. In the experiments performed here, the TP-TPBM had purities >95%, but recovery was low with >50% for HSA-IgG and 10–15% for Hb-Hp. However, a simple mathematical model used to describe the TFF purification process showed that product recovery could be increased without loss of purity by introducing TFF filters with the same MWCO in series. Taken together, this study presents a new method for selective purification of proteins using TFF and simple mathematical models to describe and predict the performance of TFF systems.

1. Introduction

Protein purification is the foundation for most of the biopharmaceuticals in the market place. The purified protein product can be used in all aspects of healthcare for applications such as therapeutics, diagnostic agents, and research [1]. Therapeutic proteins serve to supplement or restore biological function (such as plasma components) or as targeted therapies (such as monoclonal antibodies). Diagnostic proteins primarily include antibody detection systems and other bioassays used to detect markers of disease or biological dysfunction. Finally, given that research is required to validate protein usage, research proteins encompass all application areas. Moreover, in addition to the biopharmaceutical market, recent industrial use of proteins as biocatalysts has further increased the demand for proteins [2]. Thus, given the high demand for proteins, many protein purification methods have been developed over the years [1]. Unfortunately, although these new methods have reduced the overall cost of proteins, a substantial fraction of the manufacturing cost of proteins still comes from the protein purification process [1].

Most large-scale processes for protein purification rely on several chromatography steps to achieve the desired protein purity. These chromatography steps must each be individually optimized for the specific protein of interest [3]. Moreover, conventional column chromatography techniques are associated with high production costs and low volumetric throughput [4]. Thus, there have been many research efforts to develop non-chromatographic purification techniques such as protein precipitation or liquid-liquid separation [5,6]. Interestingly, membrane-based size exclusion separation methods have not been widely used for selective protein purification. Current uses of membrane filtration mainly include solution clarification (microfiltration), virus and bacterial removal, protein concentration, and buffer exchange [7]. More recent membrane separation methods have started to use both size and charge for separation (termed high-performance tangential flow filtration) [8]. However, the use of membrane-based separation for selective protein purification is still not widely used in industry.

In this study, tangential flow filtration (TFF) is used to purify a target protein (TP) from a mixture of proteins by exploiting molecular size changes that arise from the formation of a protein-protein complex

Abbreviations: TFF, tangential flow filtration; TP, target protein; TPBM, target protein binding molecule; IgG, immunoglobulin G; HF, hollow fiber; HSA, human serum albumin; RBC, red-blood cell; Hb, hemoglobin; Hp, haptoglobin; FIV, Cohn Fraction IV.

* Corresponding author.
E-mail address: palmer.351@osu.edu (A.F. Palmer).

https://doi.org/10.1016/j.memsci.2020.118712
Received 24 June 2020; Received in revised form 1 September 2020; Accepted 2 September 2020
Available online 8 September 2020

consisting of a TP and a TP binding molecule (TPBM). Previous studies have used a similar approach referred to as "affinity filtration". However, most of the studies used solid substrates that adsorbed the TP or had ligands covalently attached to the substrate that were specific to the TP [9–12]. Later studies employed water soluble polymers bound to ligands as the TPBM [9,13]. Yet, in all these systems, there was a requirement of either an insoluble affinity matrix or high molecular weight (MW) polymer conjugated to a ligand to facilitate selective binding of the TP. Our goal is to demonstrate that the range of applicable TPBMs is wider, and can consist of simple proteins capable of selectively complexing with the TP. Compared to polymer TPBMs, proteins are viable alternatives since polymers may adsorb to filter membranes, thus increasing membrane fouling, and polymeric solutions tend to have high viscosity which can decrease the flux through the membrane [14, 14–18]. More importantly, protein-based TPBMs may be engineered to have a desired MW and binding affinity to the TP for optimal performance in a proposed system.

Similar approaches have been used to isolate enantiomers from racemic protein solutions, but this practice has not been implemented for complex mixtures [19]. Moreover, micellar enhanced ultrafiltration and chelating agents can be used to bind to low MW organic or inorganic species, however this approach lacks specificity and has not been applied to large protein species. Most notably, electrostatic protein-protein interactions have been used in artificial binary protein mixtures to control protein retention (via attractive interactions) and transmission (via the Donnan effect) [20,21]. Although this concept is vital for understanding membrane-based protein separations, it lacks selectivity in isolating a specific protein from a complex protein mixture as impurities may have similar charge to the TP. Moreover, even similarly charged proteins can have attractive electrostatic interactions and the resulting complex may quickly precipitate, further complicating analysis and implementation of this method for complex mixtures [20]. Therefore, we use specific protein-binding interactions to yield a desired soluble TP complex that enables the concept of altering a TP's MW to be used in separating a TP from a complex mixture with high selectivity.

Briefly, the method employs TFF with a defined MW cut off (MWCO) membrane to first permeate the TP and other protein impurities (i.e. filtrate) that are below the MWCO of the membrane, as well as set the maximum size/MW of the protein species in the filtrate. A TPBM is then added to the filtrate to selectively create a protein-protein complex with the TP in the protein mixture that is above the MWCO of the original membrane. With only the TP-TPBM complex in the protein mixture above the MWCO of the original membrane, it can be selectively separated from the other low MW protein components in the filtrate by passing it through the original MWCO TFF membrane. TFF can then be applied to buffer exchange the complexed protein under dissociative conditions and separate the TP from the TPBM using a MWCO membrane that is between the MW of the TP and TPBM. This process is illustrated in Fig. 1.

In this study, we provide two experimental examples of using the method illustrated in Fig. 1. Moreover, we developed a mathematical model to describe and predict product recovery and purity using this method as well as to optimize the TP/TPBM pair and affinity. We further demonstrate that the model predicts that sequential staging may be used to increase the protein-protein complex recovery without loss of product purity.

2. Materials and methods

2.1. Materials

Sodium phosphate dibasic, sodium phosphate monobasic, anti-human serum albumin polyclonal antibody in immunoglobulin G (IgG) fraction of rabbit serum, and sodium chloride were purchased from Sigma Aldrich (St. Louis, MO). 0.2 μm Millex-GP PES syringe filters were purchased from Merck Millipore (Bellerica, MA). A KrosFlo®

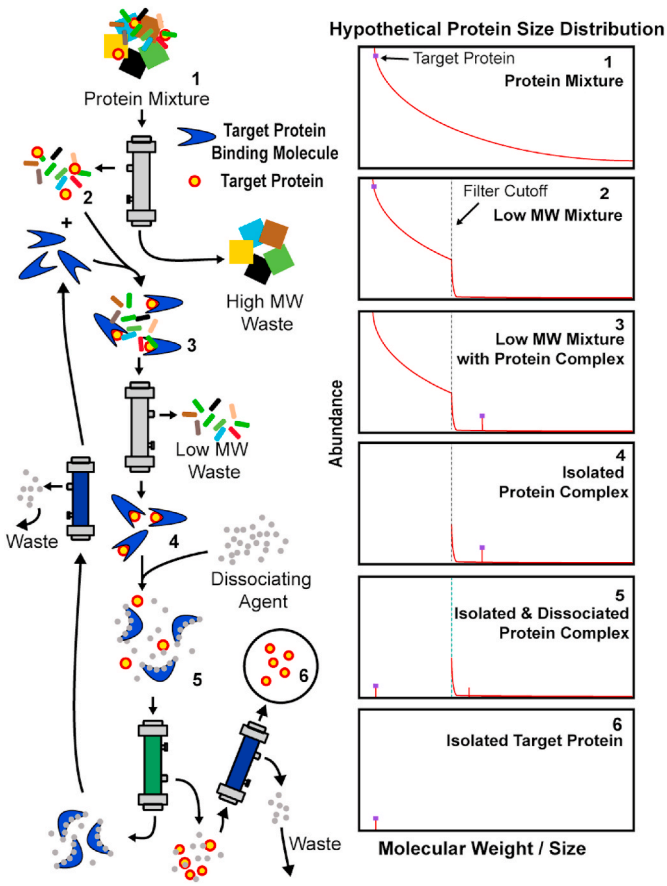

Fig. 1. Illustration of affinity ultrafiltration facilitated via protein-protein interactions. Starting with a mixture of proteins/particulates **(1)** (example: cell lysate, human plasma, etc.), the mixture is filtered through a membrane with an appropriate MWCO that permeates the TP along with low MW impurities **(2)**. Then a TPBM (i.e. antibody or equivalent, etc.) specific to the TP is introduced into the filtrate, forming a TP-TPBM protein complex that is larger than the MWCO of the original membrane **(3)**. The solution with the newly formed TP-TPBM protein complex is then refiltered through the same MWCO membrane leading to retention of the isolated TP-TPBM protein complex of interest and removal of low MW impurities **(4)**. The isolated TP-TPBM protein complex can then be dissociated to yield free TP and TPBM via appropriate buffer exchange under conditions that would facilitate their dissociation **(5)**. With the individual species (TP and TPBM) dissociated in solution, the TP can be separated from the TPBM using a MWCO membrane that is between the MW of the TP and TPBM **(6)**. Note: both the TPBM in the retentate and TP in the filtrate can be buffer exchanged via TFF into appropriate buffers to remove the dissociating agent and concentrate the separated TP and TPBM.

Research II tangential flow filtration (TFF) system and hollow fiber (HF) filter modules were obtained from Repligen (Waltham, MA). Human fraction IV paste was purchased from Seraplex, Inc (Pasadena, CA). Human serum albumin (HSA) manufactured by OctaPharma (Lachen, Switzerland) was purchased from NOVA Biologics, Inc (Oceanside, CA). Expired units of human red blood cells (RBCs) and thawed human plasma were generously donated by the Transfusion Service in the Wexner Medical Center at The Ohio State University (Columbus, OH).

2.2. Hb purification

Human hemoglobin (Hb) was purified via tangential flow filtration as described by Palmer et al. [22].

2.3. Human serum Albumin-IgG complex formation

Human serum albumin (HSA) was titrated against various concentrations of anti-HSA immunoglobulin G (IgG) and monitored for HSA-IgG complex formation via size exclusion high performance liquid chromatography (HPLC-SEC). In these mixtures, the HSA concentration was fixed at 0.08 mg/mL, while IgG varied from 0 to ~0.4 mg/mL.

2.4. Purification of HSA-IgG from artificially produced Hb and HSA mixture

HSA (0.08 mg/mL) was mixed with twice the concentration of Hb (0.16 mg/mL). Then IgG was added to the resulting protein mixture at ~2:1 mass ratio (HSA:IgG) to form the HSA-IgG complex. The resulting mixture was then subject to constant volume diafiltration on a 70 kDa hollow fiber (HF) filter (mPES, 20 cm^2, C02-E070-05-N) to retain the HSA-IgG complex (13 diafiltration volumes against phosphate buffered saline (PBS) was performed). The yield was determined based on the ratio of the area under the curve of the HPLC-SEC chromatogram at 280 nm (excluding free HSA).

2.5. Purification of HSA-IgG from human plasma

Human plasma was filtered through a 70 kDa HF filter with 15 diafiltration volumes against PBS. The permeate of the 70 kDa HF filter was concentrated on a 50 kDa HF filter (PS, 20 cm^2, S02-E050-05-N). Then, approximately 1 mg of IgG was added to the resulting mixture to form the HSA-IgG complex. The mixture was then re-filtered through a 70 kDa HF filter to isolate the HSA-IgG complex (15 diafiltration volumes against PBS). The yield was determined based on the ratio of the area under the curve of the HPLC-SEC chromatogram at 280 nm (excluding free HSA).

2.6. Haptoglobin-Hb complex purification from Cohn Fraction IV

Based on a recently developed process to purify human haptoglobin (Hp) via TFF, we employed the protein complex purification method to recover the Hb-Hp protein complex from its waste stream [23]. Briefly, 500 g of human Fraction IV (FIV) was suspended then centrifuged to remove insoluble particulates (mostly lipoproteins). The supernatant was concentrated using a 0.2 μm HF filter to 2 L. The retentate was left to rest for 36 h to flocculate low density particles, while the filtrate was kept at 4 °C for further processing. After flocculation of the retentate, low density particles in solution were separated. The higher density fraction was then subjected to 10 diafiltration volumes with PBS. The 0.2 μm filtrate was then filtered through a series of HF filters (750, 500 and 100 kDa) as previously described. Hb was then continuously added to the permeate from the 100 kDa HF filter to form the Hb-Hp protein complex, while maintaining the solution with excess Hb to bind all of the Hp in the permeate. The filtrate/Hb mixture was then subjected to 100 diafiltration volumes on a 100 kDa HF filter using fresh PBS to remove excess Hb and low MW proteins. The resulting Hb-Hp complex was then centrifuged for 30 min at 3000 g to remove any insoluble particulates that may had formed during processing. The diagram of the purification process is shown in Fig. 2.

2.7. Isolation of Hp from Hb-Hp complex

To facilitate dissociation of Hb from the purified Hb-Hp complex, 7 mL of Hb-Hp at 2 mg/mL was buffer exchanged (7 diacycles) into a 5 M urea solution at a pH 10 using a 70 kDa HF filter (mPES, 20 cm^2, C02-E070-05-N). The resulting unfolded protein mixture was then subjected to 10 diacycles using the urea solution with a rest period of 12 h in between processing to yield a total of 30 diacycles. The solution was then diafiltered for 10 diacycles into deionized (DI) water followed by 7 diacycles into PBS using a 30 kDa HF filter (mPES, 20 cm^2, C02-E030-05-N). The schematic of this process is shown in Fig. 3.

2.8. Analytical size exclusion chromatography

Hp fractions were separated via analytical size exclusion high performance liquid chromatography (HPLC-SEC) using an Acclaim SEC-1000 (4.6 × 300 mm) column (Thermo Fisher Scientific, Waltham, MA) attached to a Dionex UltiMate 3000 system (Thermo Fisher Scientific, Waltham, MA) as described previously [23].

2.9. Hb concentration

The concentration of Hb was measured spectrophotometrically using a HP 8452A Diode Array Spectrophotometer (Hewlett Packard, CA) via the Winterbourn equations [24].

2.10. Gel Electrophoresis

The purity of Hb-Hp and Hp was analyzed via SDS-PAGE using an Invitrogen Mini Gel Tank (Thermo Fisher Scientific, Waltham, MA). Samples was prepared according to the manufacturer's guidelines. Gels were loaded with approximately 30 μg of protein per lane and tested under reducing (via addition of 0.1 M dithiothreitol) and non-reducing conditions. Densitometry was performed using ImageJ.

2.11. Hb binding capacity of Hp

The Hb binding capacity (HbBC) of Hp samples was determined based on the fluorescence quenching method described in the literature using a PTI Fluorometer (Horiba Scientific, NJ) [25].

2.12. Mathematical model of TFF

A simple mathematical model was developed to describe the sepa-

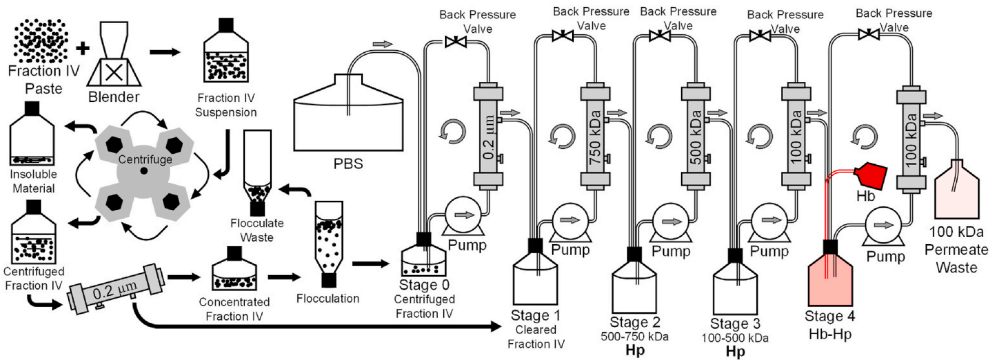

Fig. 2. General production scheme for the purification of the Hb-Hp protein complex from Cohn fraction IV paste using TFF.

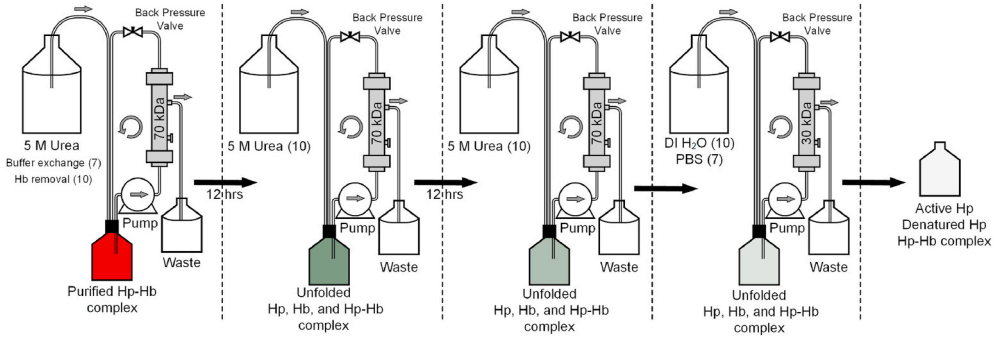

Fig. 3. Diagram showing the dissociation of Hb from the Hb-Hp complex to isolate Hp. Numbers in brackets indicate the number of diafiltration volumes.

ration of molecules via TFF. Briefly, the system (retentate vessel, TFF filter and tubing) was assumed to be well mixed (i.e. permeate flow rate was much lower than the pump flow rate, leading to negligible concentration difference between inlet and outlet of HF filter) and at constant volume (V). Furthermore, the feed flow rate (F) from the feed reservoir into the retentate vessel was assumed to be constant which, based on a constant system volume, led to the permeate flow rate (P) being equal to the feed flow rate (F). Moreover, the permeate concentration of each species was determined based on Equation (1).

$$C_{i,P} = C_{i,V}{}^{*}(1 - R_i) \tag{1}$$

In which $C_{i,P}$ is the concentration of species i in the permeate, $C_{i,V}$ is the concentration of species i in the retentate vessel and R_i is the fraction of species i retained on the membrane (i.e. retention factor). Based on these assumptions and without considering any chemical reactions, the species concentration over time was determined from Equation (2) (see Supplementary Information for derivation with reaction).

$$\frac{dC_{i,V}}{dt} = \left(C_{i,F} - C_{i,P}\right)^{*}F/_{V} \tag{2}$$

In which $C_{i,F}$ is the concentration of species i being fed into the retentate vessel and t is the process time. Normalizing the process time by the time for the completion of one diafiltration volume ($\tau = V/_{F}$), the change in concentration per diafiltration volume yields the simplified relationship shown in Equation (3).

$$\frac{dC_{i,V}}{dt_D} = \left(C_{i,F} - C_{i,P}\right) = \left(C_{i,F} - C_{i,V}{}^{*}\left(1 - R_i\right)\right) \tag{3}$$

In which t_D is the dimensionless time equal to the number of diafiltration volumes ($t_D = t/_{\tau}$). Equation (3) can be analytically solved for a system initially charged with C_{i,V_0} to yield the fraction of species i retained in the system ($C_{i,V}/C_{i,V_0}$) as shown in Equation (4).

$$\frac{C_{i,V}}{C_{i,V_0}} = \frac{C_{i,F}}{C_{i,V_0}(1 - R_i)} + \left(1 - \frac{C_{i,F}}{C_{i,V_0}(1 - R_i)}\right)e^{-(1-R_i)t_D} \tag{4}$$

To model this system, it was necessary to obtain the retention factor for each of the species being modeled (R_i). This was determined based on the manufacturer's specified retention values for TFF filters with MWCOs of 30, 50, 70 and 100 kDa. Based on these values, the Hill equation was used to model the S-shaped retention curves as shown in Equation (5).

$$R_{i,j} = \frac{1}{\left(\frac{MW_{50j}}{MW_i}\right)^{n} + 1} = \frac{1}{\left(\frac{MWCO_j + b}{MW_i}\right)^{n} + 1} \tag{5}$$

In which MW_{50j} is the MW that corresponds to 50% retention for a particular filter j, n in the Hill coefficient (i.e. steepness of the curve) and MW_i is the MW of the species i. The assumptions used to determine values for MW_{50j} and n were that all HF filters had the same Hill coefficient (n) and that the MW_{50j} for a filter was determined based on the difference between its specified $MWCO_j$ and a parameter b that was equal for all HF filters. A non-linear least squares regression was performed in Excel to determine b and n which yielded values of −12.6 kDa and 2.96, respectively. A diagram of the modeled TFF system, and the manufacturer specifications for each filter with their corresponding fitted retention curves are shown in Fig. 4.

For modeling of HSA-IgG separation, the MW of HSA was set to 65 kDa and the MW of the HSA-IgG complex was set to 220 kDa. For modeling of the Hb-Hp separation, the MW of tetrameric Hp was set to 210 kDa while the MW of the tetrameric Hb-Hp complex was set to 340 kDa.

3. Results and discussion

3.1. HSA-IgG complex purification

In the initial studies, our aim was to recover human serum albumin (HSA) using an immunoglobulin G (IgG) that was specific to HSA. Thus, based on the terminology presented in Fig. 1, HSA was the TP and IgG was the TPBM. However, to design the experiment, we first sought to characterize the HSA-IgG (TP-TPBM) complexes formed when the two components (TP and TPBM) were mixed. These results would aid in determining the MWCO of the HF filter to use for isolation of the TP-TPBM complex and what concentrations of HSA and IgG would yield the largest amount of bound HSA molecules per IgG molecule with minimal unbound HSA. Since a polyclonal IgG was used, it would be expected that at low IgG to HSA mass ratios, IgG would bind to a single HSA molecule, leading to efficient binding of HSA, but with unbound HSA still remaining in solution. Conversely, at high IgG to HSA mass ratios, all HSA molecules would be bound, but more than one IgG could bind to each HSA molecule (via binding to different epitopes on the HSA surface). Thus, the polyclonal IgG used in this study was mixed at varying mass ratios with HSA to analyze the size of the HSA-IgG complexes formed and the optimal mass ratio for HSA recovery. The resulting mixtures were then separated via HPLC-SEC and the results are shown in Fig. 5.

As shown in Fig. 5, at the concentrations used in this study, a 2:1 HSA to IgG mass ratio resulted in most of the HSA existing in an unbound state. When the mass of IgG was double that of HSA, almost all the HSA was complexed with IgG. Further, at five times the mass of IgG compared to HSA, no free HSA was detected in solution. Moreover, it was possible to note the formation of at least two distinct HSA-IgG complexes (indicated in Fig. 5A). The first eluted at ~8 min (~300–400 kDa) while the second eluted at ~7.5 min (~700–800 kDa). It was likely that these MW estimates were overestimates, since the HSA-IgG species do not have a spherically compact structure, leading to a larger overall apparent size shown in the HPLC-SEC chromatogram. Thus, it was concluded that the first complex corresponded to a single IgG molecule bound by one or two HSA molecules (~200–250 kDa), while the latter corresponded to a complex with more than one IgG molecule. Although no other distinct peaks were observed, the SEC column used in this study was limited by a

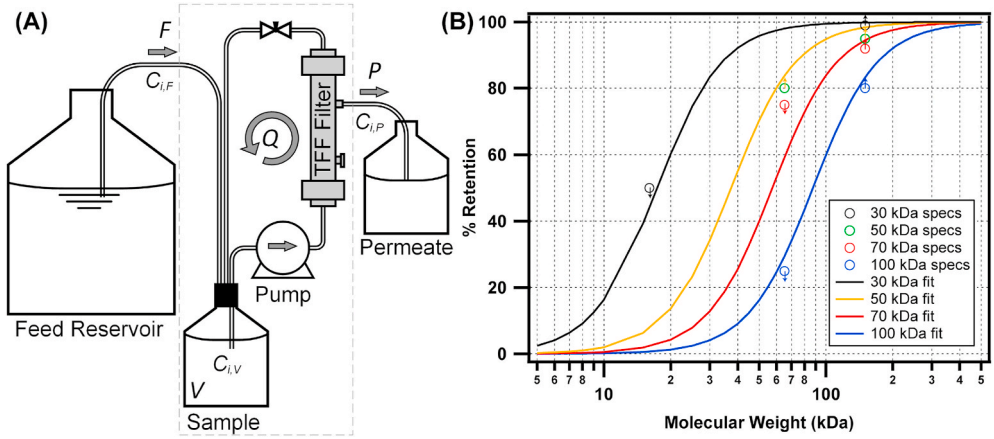

Fig. 4. Diagram of the single stage TFF system (indicated by the gray dashed lines) used for modeling the TFF process (A). Manufacturer's specifications (specs) for 30, 50, 70 and 100 kDa mPES HF filters (arrows indicate specification of more than or less than) and the fitted retention curves based on the Hill equation for each HF filter (B).

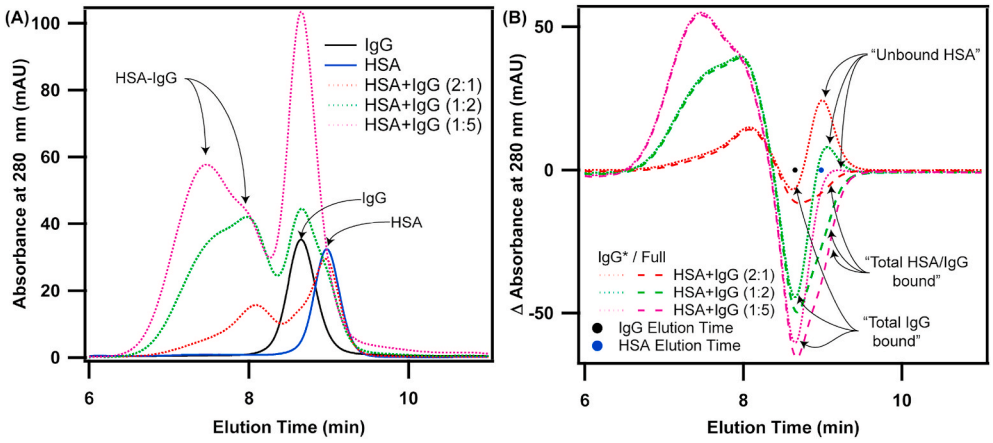

Fig. 5. HPLC-SEC of mixtures of HSA and IgG. (A) Full chromatogram with pure species. (B) Change in absorbance based on the difference between the mixture chromatogram and the pure species chromatograms. Quotation marks were used, since the difference in spectra is not a perfect description of the bound species. The HSA concentration was set to 0.08 mg/mL and approximate IgG concentrations of 0.04 mg/mL, 0.16 mg/mL and 0.4 mg/mL were employed. Numbers in parenthesis indicate the approximate mass ratio. *corresponds to the change in absorbance when only considering IgG as an initial species.

separation range of up to 1000 kDa which prevented proper separation of larger order complexes on the chromatogram, which could have also formed.

These observations agreed with the expected behavior as formation of the single IgG complex was favored when high HSA to IgG mass ratios were used, while the higher order complexes were favored when more IgG was added. Therefore, since at a mass ratio of 2:1 (HSA:IgG), most of HSA was already bound, further increasing the mass of IgG likely lead to formation of higher order HSA-IgG complexes, consuming more IgG per bound HSA. More importantly, based on Fig. 5 it was determined that the IgG-HSA complexes formed had MWs larger than at least 200 kDa (IgG-HSA complex). Therefore, it was expected that a HF module with MWCO of 70 kDa would be able to sufficiently retain the HSA-IgG complexes, while permeating HSA and small amounts of unbound IgG.

After characterizing the HSA-IgG complexes, our first step in validating the selective TFF strategy in Fig. 1 was to demonstrate the recovery of the TP-TPBM complex via IgG (TPBM) binding to HSA (TP) in an artificial mixture composed of HSA and hemoglobin (Hb). Hb (64 kDa) and HSA (66 kDa) have similar MWs (an indicator of molecular size), which imply that they could not be efficiently separated via conventional TFF. However, by using IgG as a TPBM, the HSA-IgG complex may be isolated from Hb, yielding the purified HSA-IgG complex. Hb was chosen as the impurity in HSA purification as it has a characteristic high absorption band (Soret peak) which facilitated tracking of the impurity (i.e. the Hb). In this scenario, the protein mixture was already composed of low MW species, thus pre-filtration of the mixture to retain larger MW impurities was not performed. Based on the results of Fig. 5, a ~1:2 (HSA:IgG) mass ratio was chosen to form the HSA-IgG complex, since at this ratio, most of HSA bound to IgG while the formation of higher order IgG complexes was minimized. After mixing HSA and Hb and adding anti-HSA IgG, the resulting mixture was subjected to constant volume diafiltration on a 70 kDa HF membrane to isolate the HSA-IgG complex. The results from this analysis are shown in Fig. 6.

As mentioned previously, HSA (66 kDa) and Hb (64 kDa) have similar MWs, but they differed in their elution times due to their shape (Hb is a more compact sphere compared to HSA, leading to a higher elution time). In the HPLC-SEC chromatogram, the mixture yielded an almost uniform peak (Fig. 6A and C and) when monitoring the absorbance at 280 nm. However, Hb has a strong absorbance in the Soret region, while HSA does not, easily facilitating the detection of Hb in the mixture (Fig. 6A). After addition of IgG to the mixture, the HSA-IgG complex was formed (Fig. 6C). Moreover, the initial permeate from the diafiltration process was found to contain primarily Hb as the 280 and 413 nm peaks overlapped (Fig. 6B). On the other hand, after 13 diafiltration volumes, the permeate was practically cleared of Hb with minimal amounts of protein permeating through the filter. Thus, as shown in Fig. 6C, the final isolated HSA-IgG complex contained no detectable level of Hb.

In addition to confirming that no detectable levels of Hb was present, based on the overall recovered HSA-IgG complex chromatogram, more than 50% of the complex was recovered. Unfortunately, some of the >200 kDa species were lost, which would not be expected to easily

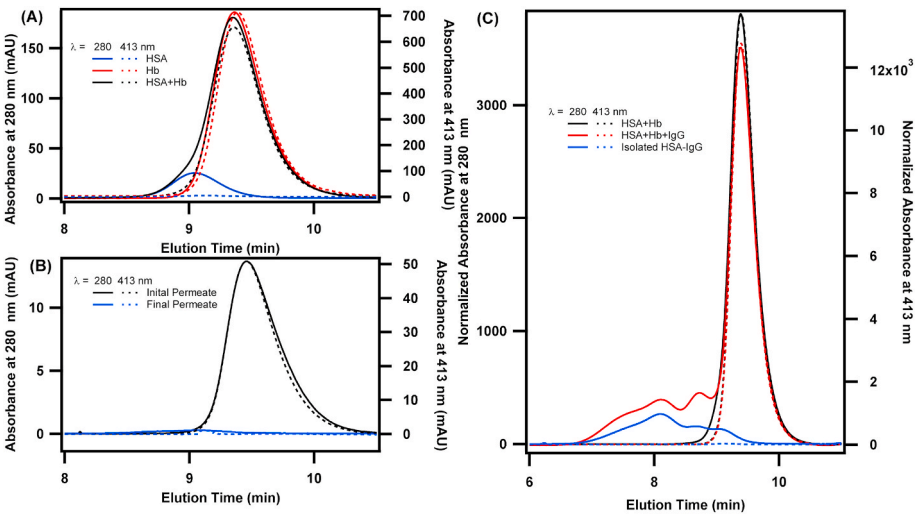

Fig. 6. Purification of HSA-IgG complex from artificially produced HSA and Hb mixture. (A) HPLC-SEC of HSA, Hb and mixture of HSA and Hb. (B) HPLC-SEC of first and last permeates of 70 kDa HF filter. (C) HPLC-SEC of initial HSA and Hb mixture before and after IgG addition and isolated HSA-IgG complex. Normalization accounted for the different total volume of samples.

permeate through the 70 kDa HF filter. These species were likely lost either through general processing (unspecific binding to the filter, or retained in the tubing) or some of the HSA-IgG complexes may have precipitated (either due to TFF processing or via aggregation of large immune complexes). Moreover, the equilibrium between the HSA-IgG complex and unbound proteins could have contributed to the loss of HSA and some IgG since the dissociation constant of rabbit polyclonal anti-HSA IgG has been shown to be on the order of 10^{-8} M which is almost of same order of magnitude as the concentration of IgG used in this study (10^{-7} M) [26]. Moreover, the heterogeneity of polyclonal antibodies can lead to dissociation constants ranging from 10^{-4} M to 10^{-12} M. Thus, the HSA-IgG complex in equilibrium with unbound HSA and IgG may have continuously shifted towards the unbound components as HSA was filtered out of the system, thus reducing the amount of HSA-IgG complex [27].

Even though the retained HSA-IgG complex on the SEC-HPLC chromatogram showed the presence of low MW species that would be expected to permeate through the 70 kDa HF filter, based on the low protein content of the permeate, further diafiltration was ineffective. In this experiment, the protein load on the membrane was low, thus fouling of the membrane was unlikely. Thus, the presence of these low MW species in the chromatogram may be due to the dissociation of the complexes in equilibrium with the individual proteins in the complexes, while running them on the HPLC-SEC column [28–31]. As mentioned above, this dissociation may have been favored due to the low concentrations of IgG used. Further, even though the antigen-antibody reaction favors complex formation, it has been shown that, depending on the dissociation rate constant, it is possible for the complex to dissociate during analysis in the SEC column [31,32]. Finally, filtration of the same HSA and Hb mixture through the 70 kDa HF filter without addition of IgG lead to permeation of practically all the protein within ~10 diafiltration volumes. Thus, the HSA-IgG complex could not be further purified.

Overall, in this first experiment, we successfully isolated HSA-IgG from a simple mixture of HSA and Hb (Fig. 6). Next, we sought to demonstrate how to purify a protein in its complexed form from a complex mixture. Since we had already demonstrated separation of HSA-IgG, we used the same TP and TPBM pair to isolate HSA-IgG from plasma, a complex protein mixture. Unlike the simple HSA and Hb mixture, plasma contained large MW impurities. Thus, plasma was first diafiltered on a 70 kDa membrane to permeate HSA while retaining large MW species (i.e. permeating the TP and low MW impurities). The permeate fraction from the 70 kDa membrane was concentrated on a 50 kDa HF filter to maintain a constant operating volume, forming a fraction between 70 and 50 kDa (bracket between permeate of 70 kDa HF filter and retentate of 50 kDa HF filter: 70P-50R). Then, IgG was added to the 70P-50R fraction to form the HSA-IgG complex, yielding a mixture of HSA-IgG complex and low MW impurities. The HSA-IgG complex was then selectively retained by subsequent diafiltration on the 70 kDa membrane. The results from this experiment are shown in Fig. 7.

As shown in Fig. 7, plasma is a complex protein mixture with a wide range of MWs. Filtration of plasma through the 70 kDa HF filter retained most of the large MW species since plasma contained species at ~8 min elution time that were not present on the 70P-50R sample. Addition of IgG to 70R–50P led to the formation of HSA-IgG complexes with a

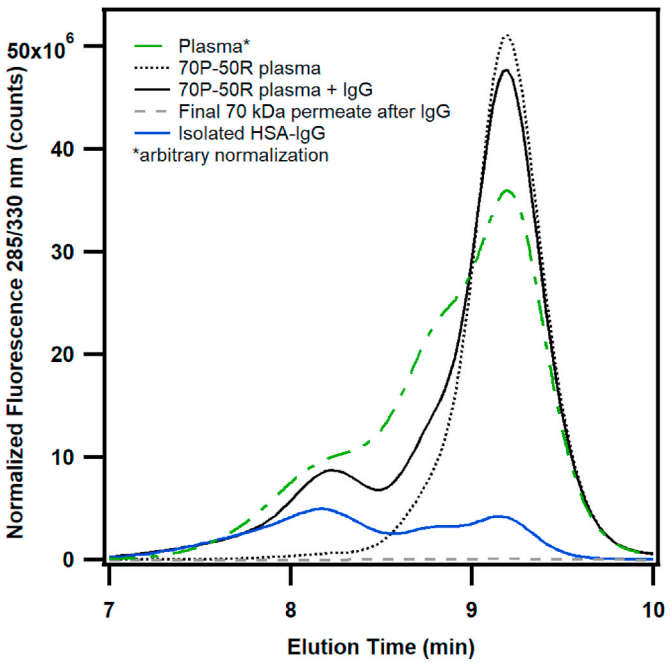

Fig. 7. Purification of HSA-IgG complex from plasma. 70P-50R represents the fraction of plasma that permeated through the 70 kDa HF filter and was retained on a 50 kDa HF filter. Normalization was used to account for different total volumes of samples.

similar elution chromatogram to that of the 2:1 (HSA:IgG) mass ratio shown in Fig. 5. This was expected as the amount of IgG added was much lower than the expected mass of HSA in the permeate.

Similar to the example demonstrating isolation of HSA from the Hb and HSA mixture (Fig. 6), ~50% of the complex was recovered. Moreover, compared to Fig. 6, a similar HSA-IgG chromatogram was observed since there were small MW species expected to permeate through the 70 kDa HF filter that appeared in the final HSA-IgG chromatogram. However, similar to the experiment in Fig. 6, practically no protein permeated through the filter as shown in the final permeate chromatogram in Fig. 7. To ensure that filter fouling was not the cause for retention of these species, the filter was cleaned with 0.1 M sodium hydroxide prior to re-diafiltering the complex. Moreover, even when a new filter was used, there was not significant removal of protein from the retained HSA-IgG complex. Thus, it was likely that the complex dissociated as it passed through the analytical HPLC-SEC column or that the HSA-IgG equilibrium allowed for the presence of pure HSA in solution.

Overall, with the HSA-IgG complex purification scheme, it was demonstrated that the protein complex TFF method could be used to isolate protein complexes. The products had high purities (based on the absence of Hb or lack of protein permeation through the HF filter), but protein complex recovery was limited by the dissociation of the HSA-IgG complex during processing. Moreover, for isolation of pure HSA, HSA could be dissociated from the HSA-IgG complex as previously described in the literature via the use of chaotropic agents or low pH incubations [27,33]. Unfortunately, we were limited by the amounts of HSA-IgG used in this study and, therefore, did not replicate the methodologies described previously. Nonetheless, these initial experiments illustrated the basics of the protein complex purification strategy via TFF.

3.2. Hb-Hp/Hp purification from Cohn Fraction IV

After assessing that protein complexes could be purified with the methodology described in this study, we next sought to test this purification strategy using a practical example. In our lab, we purify large amounts of Hb and Hp using TFF [22,23]. Hp is a plasma glycoprotein with the main role of scavenging toxic cell-free Hb in blood. During conditions in which red blood cells lyse (i.e. hemolysis), plasma Hp quickly binds to Hb, preventing the toxic side-effects of cell-free Hb. However, during extensive hemolysis, plasma Hp levels are depleted, allowing cell-free Hb to elicit oxidative tissue damage and systemic hypertension. Therefore, Hp replacement therapy may be used to treat these states of hemolysis by binding to cell-free Hb in plasma to detoxify it. However, in the Hp purification process, approximately 50% of Hp initially present in human Cohn fraction IV (FIV) is lost as it is not retained within the TFF system. Thus, we wanted to recover this Hp via the selective TFF method described in this work. Moreover, with the large volumes of Hp and Hb being processed, we were able to perform dissociation studies to separate Hb and Hp from the Hb-Hp complex, to prove that we can recover the individual proteins (Hb and Hp) from the Hb-Hp protein complex.

As shown in Fig. 2, the last HF filter used for Hp purification has a MWCO of 100 kDa. In this scenario, the Hp purification process retained any large MW impurities from FIV, leaving only Hp and low MW impurities on the 100 kDa permeate. Given the high binding affinity of Hp for Hb, Hb was used as a TPBM to bind to Hp (the TP) that permeated through the terminal 100 kDa filter of the Hp purification process. Then the Hb-Hp containing permeate was re-diafiltered through a 100 kDa HF filter to isolate the Hb-Hp complex. Similar to isolation of HSA-IgG from the HSA and Hb mixture, use of Hb as the TPBM has the advantage of possessing a Soret peak which allows for tracking of the Hb-Hp complex. Moreover, the Hb-Hp complex itself has potential biomedical applications given that it could be used to target CD163+ macrophages and monocytes [34,35].

Based on this idea, excess Hb was added to the 100 kDa permeate of the process used to isolate Hp (Fig. 2) described in the **Methods Section** to form Hb-Hp complexes. Then, the Hb and permeate mixture containing Hb-Hp was refiltered through a 100 kDa filter to isolate the Hb-Hp complex. Dissociation of the complex was later performed using 5 M urea as the dissociating agent, which allowed for partial removal of Hb from Hb-Hp. The overall procedure used in this experiment is illustrated in Fig. 8.

During the purification of the Hp-Hb complex, samples were taken at different stages of the process. These samples were analyzed on an HPLC-SEC column and the results were compared to the theoretically predicted separation based on the schematic in Fig. 1. The comparison of predicted versus experimental results are shown in Fig. 9.

From these results, the addition of Hb to Cohn Fraction IV increased the amount of large MW species (compare 1 to 1*). These species matched our purified product (compare 1* to 4). Furthermore, permeate analysis (2) showed that the unbound Hp did not easily permeate through the 100 kDa HF filter. This can be seen due to a lower relative abundance of the Hb-Hp complex when Hb was added to the protein mixtures (compare the amount of Hb-Hp in 1* to 3). Another observation was that, by comparing 2 to 4, it was noticeable that some of the Hb-Hp complex was capable of permeating through the 100 kDa HF filter. This was not surprising as Hb only added 64–96 kDa to the low MW Hp species (dimers and trimers). Thus, the change in MW from Hb binding was not sufficient for full retention of the complex on the 100 kDa membrane. Yet, even though some of the complex was lost, we were able to isolate some of the Hb-Hp and demonstrate the application of this purification strategy. Moreover, based on the purified complex elution time, the Hb-Hp complex had a MW of ~350 kDa which indicated it was an average of ~220 kDa for the pure Hp (approximate MW for

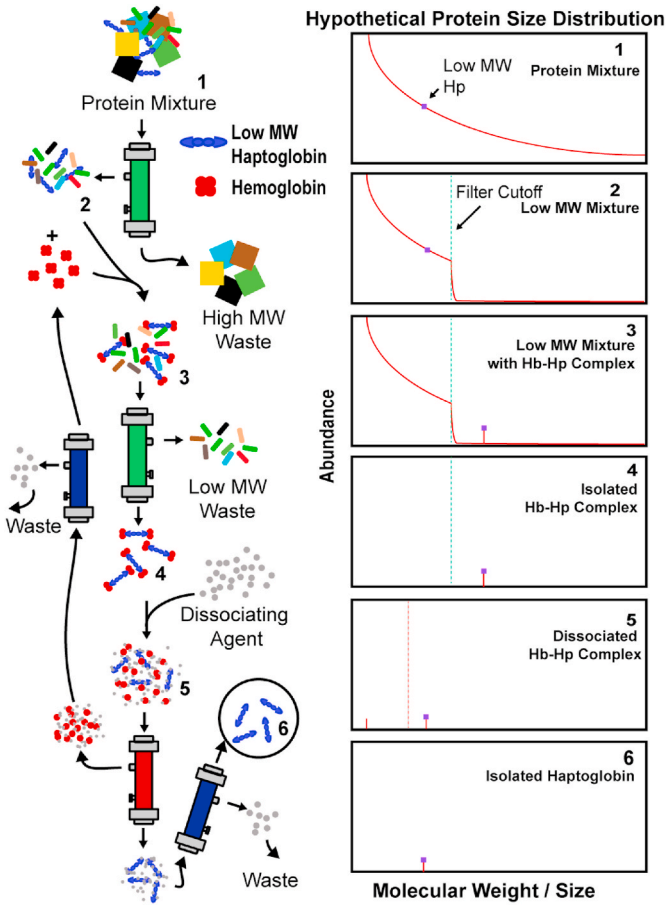

Fig. 8. Illustration of using the protein complex affinity purification method to isolate Hp from a complex mixture (the complex mixture consisted of Cohn Fraction IV and the dissociating agent was urea).

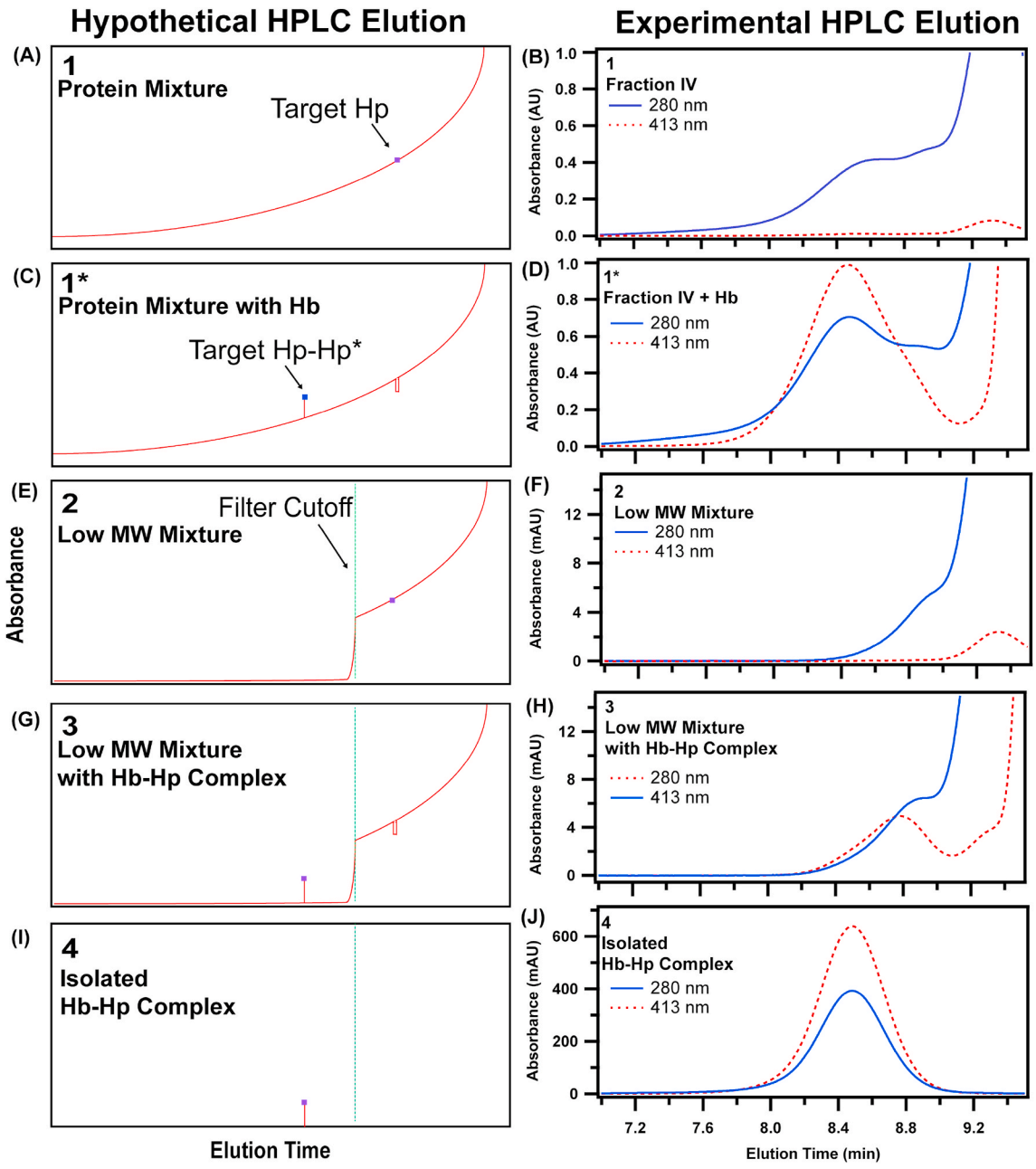

Fig. 9. Comparison of the hypothetical and experimentally measured HPLC-SEC elution chromatogram at each stage of the Hb-Hp purification process. Human Cohn Fraction IV was used as source of Hp (the TP) and after filtering the protein mixture through a 100 kDa TFF module, Hb was added as a TPBM to form the Hb-Hp complex (TP-TPBM) and the sample was re-filtered through the original 100 kDa TFF module. Hypothetical (A) and experimental HPLC-SEC (B) protein elution chromatogram for Stage 1 (protein mixture). Hypothetical (C) and experimental HPLC-SEC (D) protein elution chromatogram for Stage 1* (protein mixture and TPBM). Hypothetical (E) and experimental HPLC-SEC (F) protein elution chromatogram for Stage 2 (low MW mixture). Hypothetical (G) and experimental HPLC-SEC (H) protein elution chromatogram for Stage 3 (low MW mixture and TPBM). Hypothetical (I) and experimental HPLC-SEC (J) protein elution chromatogram for Stage 4 (isolated TP-TPBM complex).

tetrameric Hp without any bound Hb) which indicated that most Hp trimers and dimers were lost during filtration.

Using this method, the resulting Hb-Hp complex isolated contained 200 mL of 2.2 mg/mL Hb as determined from its Soret peak absorbance. Based on the expected Hb binding capacity present in the 100 kDa permeate stage of the Hp purification process (~3 g), the recovery of Hp was approximately 10–15%. The low recovery rate was attributed to the loss during general processing and from loss of product that permeated through the 100 kDa HF filter. The equilibrium between the Hb-Hp protein complex and the individual protein components (Hb and Hp) in the complex was not expected to be a factor during the separation, since the Hb-Hp complex has a dissociation constant in the picomolar range [36,37].

Starting with the purified Hb-Hp complex, Hb was dissociated as described in the **Methods Section** to isolate Hp (Fig. 3). The SDS-PAGE of the purified Hb-Hp complex and recovered Hp from the complex is shown in Fig. 10.

From the SDS-PAGE analysis, practically no impurities could be detected (>95% pure based on densitometry) in the purified Hp-Hb complex. The purification process effectively removed the low MW impurities and retained only the Hp polymers (compare Lane 4 to 1). Furthermore, from both the SDS-PAGE band intensity analysis and the

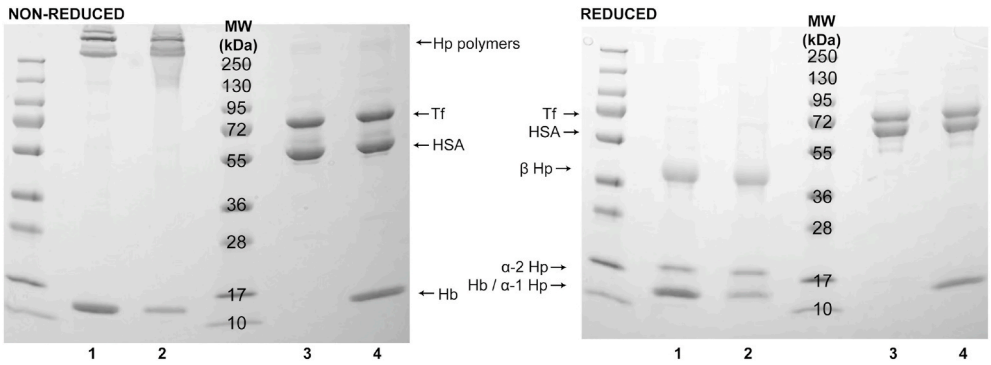

Fig. 10. SDS-PAGE of the purified Hb-Hp complex and mixture of Hp and Hp-Hb obtained from dissociation and separation of Hb from the purified Hb-Hp complex. Lane 1: Isolated Hb-Hp complex. Lane 2: Mixture of Hp and Hb-Hp. Lane 3: 100 kDa permeate. Lane 4: 100 kDa permeate with added Hb. Abbreviations: transferrin (Tf); haptoglobin (Hp), human serum albumin (HSA), hemoglobin (Hb), beta chain of haptoglobin (β Hp), alpha chain of haptoglobin (α Hp).

spectrophotometrically determined amount of Hb bound to the purified Hp species, the Hp to Hb mass binding ratio was estimated to be ~1.6:1. This is approximately the same theoretical mass binding ratio assuming one Hp2-2 dimer (expected to be the predominant Hp phenotype in Cohn Fraction IV) is bound to one Hb αβ dimer. Moreover, as shown on the SDS-PAGE most of the Hp that permeated through the 100 kDa consisted of ~250 kDa Hp polymers, which was similar to the HPLC-SEC estimates of ~220 kDa from Fig. 9.

Urea treatment of the Hb-Hp complex provided experimental proof of principle that the protein complexes could be dissociated to yield the isolated TP. Unfortunately, urea treatment was not successful in fully removing the bound Hb in the Hb-Hp complex as shown by the presence of residual Hb in Lane 2 of the SDS-PAGE. Yet, it was possible to note a decrease in the Hb band intensity in the urea treated Hb-Hp complex. Furthermore, using the 1.6:1 (Hp:Hb) mass binding ratio, SDS-PAGE analysis indicated that about 20% of the Hp was still bound to Hb as the Hp-Hb complex. In comparison, using total protein and spectrophotometric analysis, the product consisted of 25% active Hp (based on fluorescence Hb binding assay), 29% Hb-Hp complex and 52% inactive Hp (denatured). Furthermore, compared to the starting Hb-Hp complex, 52% of Hp was lost during processing, 12% was active, 13% remained bound to Hb and 23% was denatured. Overall, these results could be greatly improved through optimization of the protein unfolding conditions to avoid protein denaturing and using a lower MWCO HF filter for the diafiltrations to avoid loss of protein. However, the process to obtain the purified Hp exemplifies how to use TFF for isolation of a TP from the TP-TPBM complex.

3.3. Mathematical modeling

In order to better understand and predict the performance of the TFF separation process, the retention curves for the 70 and 100 kDa HF

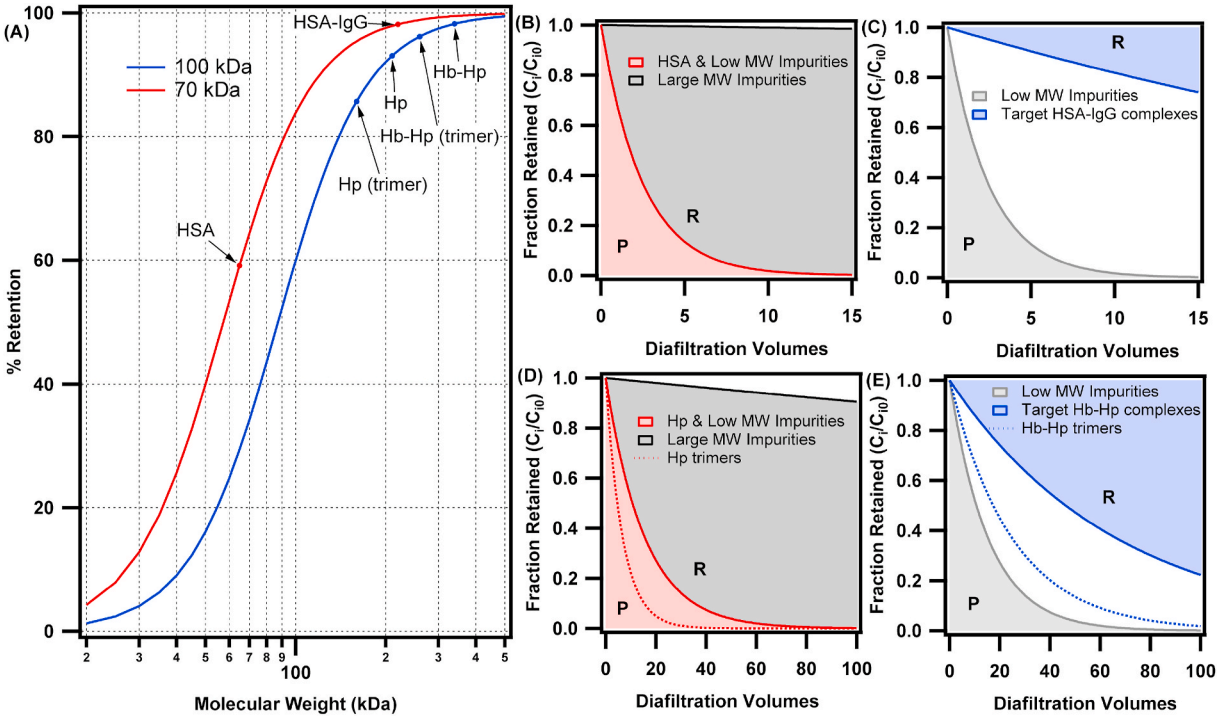

Fig. 11. Model results for the experiments performed earlier in this study. (A) Estimated retention curves and the expected retention for the species used in these studies. (B) Separation of HSA and low MW species from large MW impurities using a 70 kDa HF filter. (C) Separation of HSA-IgG complexes from low MW species using a 70 kDa HF filter. (D) Separation of Hp (tetramers and higher order Hp species, as well as trimers indicated by the dotted line) and low MW species from large MW impurities using a 100 kDa HF filter. (E) Separation of Hp-Hb complexes (tetramers and higher order Hp species, as well as trimers indicated by the dotted line) from low MW impurities using a 100 kDa HF filter. Shading indicates the range of curves that could comprise the permeate (P) and retentate (R).

filters were estimated and the simple mathematical model discussed in the **Methods Section** was employed. The results from the mathematical model for the two separation experiments performed earlier are shown in Fig. 11.

TFF filters have a nominal MWCO which rates performance of the filter for purification of different sized macromolecules. This MWCO is determined based on the retention curve of each filter (Fig. 11A). These retention curves relate the MW of the species to their percentage retention on the HF membrane. This curve is only an estimate, since the main determinants for filtration are the size and shape of the molecules, not the species mass. However, for modeling of the filtration system, estimates for the retention of the species to be separated were required. Thus, we used the manufacturer's specific retention ratings for various membranes (30, 50, 70 and 100 kDa mPES filters) to determine the best fit coefficients to the Hill equation. The Hill equation was chosen as it provides a good fit to the characteristic sigmoidal shape of membrane retention curves on a logarithmic axis [38,39]. The fits for all retention curves and description on how the retention curves were determined can be found in the **Methods Section** (Fig. 4).

Based on the retention curves, the TFF systems used for isolation of HSA-IgG (Fig. 11B and C and) and Hb-Hp (Fig. 11D and E and) were modeled. As shown in Fig. 11B, ~10 diafiltration volumes were required to permeate all (>99%) HSA through a 70 kDa HF filter which was observed experimentally when only HSA and Hb were mixed. Moreover, Fig. 11C demonstrated how the current MWCO filter led to loss of the HSA-IgG complex, which explains some of the protein loss observed experimentally. Yet, from the model, it was expected that >75% of the HSA-IgG would be retained, but only ~50% was retained experimentally. This difference was likely due to the equilibrium between the HSA-IgG complex and pure HSA and IgG species which this simple model did not account for (the effect of reaction equilibrium is further discussed later in this section).

For the isolation of Hb-Hp, the model demonstrated how trimeric Hp-Hb would not have been retained over the 100 diafiltration volumes performed (Fig. 11E). This confirmed the experimental results which indicated that tetrameric Hp consisted of most of the retained Hp. Furthermore, a substantial loss of protein was observed for the Hb-Hp complex, with only ~20% retained at the end of processing (based on the MW of tetrameric Hp). This value was in close agreement to the experimental value of 10–15%. Moreover, the model did not account for the processing required to obtain the 100 kDa Hb-Hp permeate. During the Hp purification process, Stage 3 (Fig. 2) was diafiltered for 100 diafiltration volumes which yielded a large volume of permeate. Thus, to maintain a constant volume system in Stage 4, Hb was continuously added and the mixture was diafiltered on a 100 kDa HF filter. The filtration performed during this time did not count towards the 100 diafiltration volumes performed on the Hb-Hp complex shown in Fig. 11. Thus, the additional diafiltration volumes would add ~10–20 more diafiltration volumes to the Hb-Hp complex purification, explaining why the model predicted a higher retention that what was observed experimentally. The accuracy of the model predictions without inclusion of the equilibrium reactions was likely due to the practically irreversible reaction of Hb to Hp [40], with dissociation constant much lower than that of an immunoglobulin binding to its antigen ($<10^{-12}$ M [36,37] for Hb-Hp compared to $\sim10^{-8}$ M for an antigen-antibody).

The difference in the number of required diafiltration volumes for separation of the complex from the impurities or TP can be visualized on the retention curve. For the HSA-IgG process, HSA was found close to the middle portion of the retention curve while HSA-IgG was at >90% retention. This allowed for effective permeation of HSA or low MW impurities without loss of the protein complex. On the other hand, both Hp and Hb-Hp complex were observed at >90% retention, which made it difficult to permeate the molecules. Interestingly, even in this case, we were able to experimentally purify the Hb-Hp complex. Optimal scenarios would have the TP and TPBM at the two opposing extremes of the sigmoidal retention curve, allowing for filtration of the TP and low MW impurities while retaining the TP-TPBM complex.

The model presented here also demonstrated how some of the large MW species could contaminate the isolated protein complex. Even though these large MW species would have high retention (assumed to be 99.9% retained in the model), at a sufficient number of diafiltration volumes, they could permeate significantly thorough the filter prior to the addition of the TPBM. However, for systems such as HSA-IgG in which the TP is smaller than the TPBM, dissociation of the TP-TPBM complex and separation of the TP from the TPBM would leave the impurities retained with the TPBM. Moreover, in general cases that do not require many diafiltration volumes, only small amounts of large MW complexes would be expected to permeate the filter. Furthermore, if a sufficiently large TPBM is utilized, then a larger MWCO HF filter relative to the MWCO used to permeate the TP can be used to retain the TP-TPBM complex. Thus, the large MW species (relative to the first MWCO HF filter) mixed with the TP-TPBM complex could permeate through the HF filter, leaving only purified TP-TPBM protein complex in the retentate.

In addition to assessing the specific TP and TPBM pairs discussed in this work, the simple mathematical model can predict the performance of the separation system on different TP and TPBM pairs. For example, using IgG to capture a ~20 kDa protein and using a 50 kDa HF filter for TFF could facilitate permeation of the TP and low MW impurities in 7 diafiltration volumes (less than 0.2% remaining of TP and low MW impurities) while retaining more than 90% of the TP-TPBM complex. Based on the number of amino acids present in FDA approved therapeutics [41] and assuming an average MW of ~120 Da for an amino acid, this TP-TPBM pair could be used on more than one third of FDA approved therapeutic proteins.

However, as demonstrated by the difference in the experimentally observed retention of the HSA-IgG pair compared to the model prediction, the model prediction would not provide accurate quantitative results unless the TP-TPBM complex had sufficiently high affinity to prevent dissociation under the conditions used during the separation. Thus, the dissociation and association reactions of the TP-TPBM pair can be added to the model by including a reaction term in Equation (2) (the derivation of which is described in the Supplementary Information document). Unfortunately, inclusion of the reaction term prevented the derivation of an analytical expression, requiring the use of an ordinary differential equations solver to find the solution. Moreover, the solution was dependent on the time to complete a diafiltration volume in addition to the reaction terms. Nonetheless, the results become more descriptive of a real system in which dissociation and association are occurring. The results using this more descriptive model on the separation of HSA from an artificial mixture of HSA and Hb is shown in Fig. 12.

As shown in Fig. 12, it was clear that the chemical reactions influenced the system performance, since the semi-log plots (Fig. 12B) would only exhibit linear concentration profiles for a purely filtration-based separation (note the Hb concentration profile). Comparing Figs. 12A to 11C shows that the chemical reactions caused a significant reduction in the concentration of the complex during TFF processing compared to filtration alone without accounting for the equilibrium. This additional loss of the HSA-IgG complex occurred due to complex dissociation into free IgG and HSA as the filtration process reduced the concentration of HSA in solution. Dissociation of the IgG-HSA complex is apparent due to the increase in the concentration of free IgG. Moreover, due to the dissociation of the complex, at the end of processing, the concentration profile of HSA began to asymptote to a non-zero value as the rate of protein permeation was compensated by the rate of dissociation of the complex. This final equilibrium between the protein components in the mixture agreed with the experimentally measured HPLC-SEC chromatogram. Furthermore, the model predicted that the lack of HSA permeation though the 70 kDa filter that was observed in the experiment was likely due to the protein concentrations in the permeate reaching the lower limit of detection of the HPLC system. More importantly,

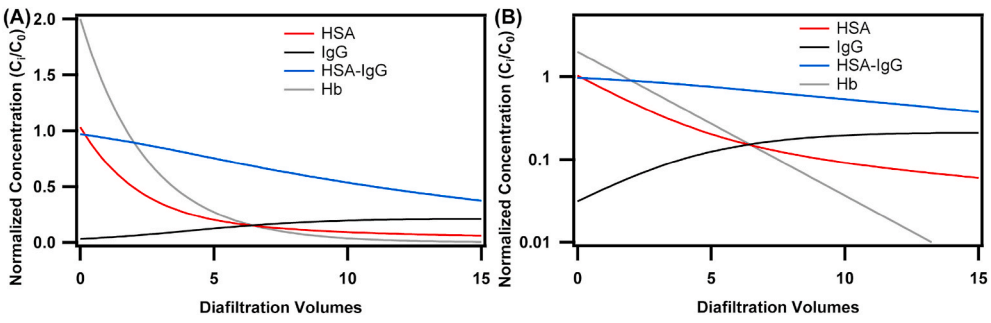

Fig. 12. Model results with association and dissociation reactions included for the initial HSA-IgG recovery from artificial HSA and Hb mixture experiment. (A) Concentration profile of species (IgG, HSA, Hb and IgG-HSA complex) assuming a single IgG species. (B) Semi-log plot of species concentration assuming a single IgG species. The model parameters used included a reference initial concentration of $3*10^{-7}$ M (C_0), time to complete a diafiltration volume (τ) of one hour, dissociation constant (K_D) of 10^{-8} M and rate of association constant of 10^6 M^{-1} s^{-1} (value obtained from the literature [42]). The initial normalized concentrations used were 2, 1 and 2 for HSA, IgG and Hb, respectively. The HSA-IgG complex was assumed to have a MW of 220 kDa, in order to determine its retention on the TFF filtration system.

based on the more descriptive TFF separation model including chemical reactions, the mass-based yield of non-HSA protein components at 15 diacycles was approximately 50% of the starting value, which was close to the experimentally measured value, indicating that, by including the reaction terms, the model showed some predictive capabilities even when association and dissociation reactions were occurring.

A potential drawback with the method being discussed here is the low protein-protein complex recovery. Yet, even though the process conditions may require many diafiltration volumes to ensure high product purity, one could implement TFF staging to increase overall protein-protein complex recovery without loss of purity. To demonstrate this, we used the mathematical model to demonstrate the enhanced product recovery based on a simple staged TFF setup in which the permeate of the first system is the fed to the second system and the permeate of the second system is fed to the third system as shown in Fig. 13.

To simplify the results, we used the model without chemical reactions although reactions could be added as described previously. The results of this analysis for the experimental conditions analyzed in this study (HSA-IgG and Hb-Hp complexes) for a three stage TFF system are shown in Fig. 14 (derivation of the mathematical equations used to determine the concentration profiles for the three stage TFF system can be found in the Supplementary Information section).

From the results shown in Fig. 14A and B, the first stage had the same concentration profile as in Fig. 11C and E, respectively. This was expected as the model in Fig. 11 was the same as a one stage system. Moreover, comparing Fig. 14A and B, it was noticeable that both systems had the same overall concentration profiles. The first stage had a decay in concentration of both species while both sequential stages had an intermediate increase followed by a decay of low MW species. Furthermore, for the target complexes, the general trend was for stages 2 and 3 to increase in concentration, but at sufficiently high number of diacycles, the concentration of Hb-Hp began to decrease. More importantly, as shown in Fig. 14C and D, use of additional stages led to an overall increase in product recovery without loss of product purity which can be achieved over the same number of diafiltration volumes (i.e. same amount of time).

Although TFF staging has been previously shown to increase overall separation efficiency, most studies have implemented complicated configurations to increase product purity and recovery [43]. Based on our model, a simple configuration of TFF modules in series allows for improved TP-TPBM product recovery without loss of product purity. A similar approach has been used combined with affinity ultrafiltration to recover permeated TP molecules that did not bind to TPBM in the first stage [44]. Although the model can describe the overall TFF system performance, it did not consider some important factors that can influence TFF processes. Mainly, there was no effect of concentration polarization on the membrane or membrane fouling which can greatly increase protein retention within the filter during processing [45]. Moreover, for these results, we assumed that the binding of the TP to the TPBM was irreversible, without consideration of protein-protein equilibria.

It is noteworthy that, with staged separation, the model predicts that the protein-protein complex may be recovered at almost any desired

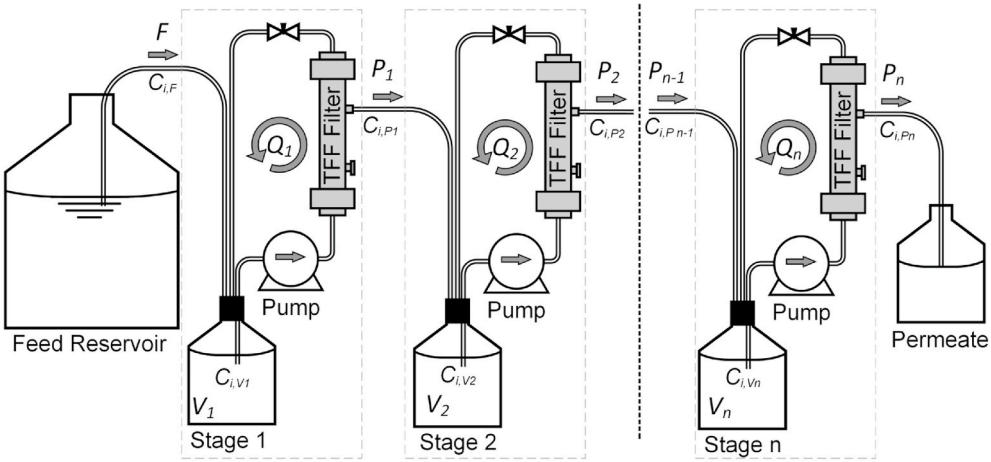

Fig. 13. Model diagram using individual TFF modules staged in series.

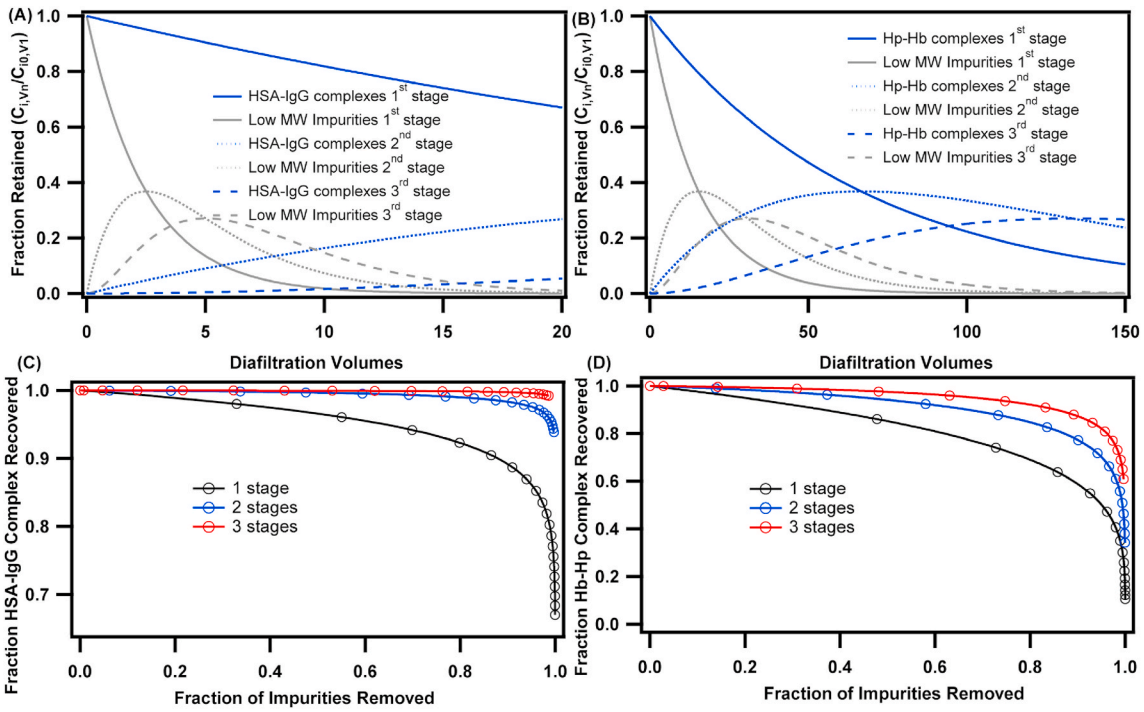

Fig. 14. Model results using individual TFF modules staged in series. (A) Serial staging of TFF modules for HSA-IgG recovery. (B) Serial staging of TFF modules for Hb-Hp complex recovery. The retained species are at or above the curves for the complexes, while the permeated species are at or below the curves for the low MW impurities. (C) Trade-off between retention of the HSA-IgG complex and removal of impurities using one, two, or three staged TFF systems (distance between each circle corresponded to 1 diafiltration volume). (D) Trade-off between retention of the Hb-Hp complex and removal of impurities using one, two, or three staged TFF systems (distance between each circle on the same curve corresponds to 10 diafiltration volumes).

purity level. However, the final TP purity would be limited by the difference in retention between the TPBM and the TP on the specific HF filter used to facilitate the separation. Moreover, although in Fig. 14, the system was assumed to contain only a single impurity of MW equal to the TP, the process is robust for various MW impurities. For example, large MW impurities (i.e. larger than the TP-TPBM complex) would be primarily retained within the high MW waste during the initial filtration of the crude material whereas the TP and low MW species would permeate through the membrane. Further, any small quantities of large MW species permeated during the initial crude filtration step would later be retained during the separation of the TP from the TPBM. Furthermore, any species with MW smaller than the TP can be removed through the staging system shown in Fig. 13. Finally, any species within the size range spanning the TP to the TPBM would be the most difficult impurities to separate. However, these impurities should not be present at high levels, since the initial filtration of the crude material should retain a large fraction of these impurities. Furthermore, these intermediate MW species could also be removed through the staging strategy shown in Fig. 13 and then partially retained during the separation of the TP from the TPBM.

Furthermore, the selective protein purification system that is described in this work may have large buffer usage requirements as demonstrated in the Hb-Hp complex example. Therefore, buffer recycling could be implemented to reduce overall buffer usage in the process [46]. Moreover, in semi-batch operation with a constant upstream feed of proteins, a significant build-up of retained species especially at the first filtration step could limit the performance of the TFF modules arranged in series. Thus, bleeding of the retentate may improve the performance of the semi-batch process. Therefore, these limitations could be addressed using more recent TFF designs that facilitate continuous protein purification [43,47–49].

Future studies could aim at using existing recombinant protein technologies to create dissociable protein complexes. For example, various tags are currently used in column affinity chromatography that could be attached to a large MW protein, forming a custom TPBM. These tagged TPBMs could lead to development of platform purification technologies using the affinity ultrafiltration approach presented here. Further, the reaction model presented could guide the design of the TPBMs binding affinity and size to ensure optimal operation of the separation process. Given that membrane filtration is already widely used for various steps in protein purification schemes, use of TFF for purification could simplify the overall production process by reducing the variety of separation equipment. Moreover, the linear scalability of TFF provides a major advantage compared to alternative purification methods as successful small-scale research systems can be easily scaled to meet market demand [50]. Further, the costs associated with this purification process may be lowered by using impure TPBM as the source of binding molecule. This could be implemented by first filtering the TP in a complex mixture over a defined MWCO membrane and using this same MWCO membrane to filter the impure TPBM. The two permeate fractions would then be mixed to yield the TP-TPBM and the low MW impurities in the mixture that could be removed by re-diafiltering through the same MWCO filter.

4. Conclusion

The study presented here demonstrates the use of protein-protein complexes (TP-TPBM) to purify proteins of interest (TP) using TFF. Preliminary experiments show that this separation strategy can be used to process complex mixtures yielding product (TP-TPBM) purities >95%. However, the separation examples used in this work exhibited low protein recoveries. Fortunately, we show that a simple mathematical model can be used to guide the application and optimization of this purification strategy even when there are dissociation and association reactions between the TP-TPBM complex and the individual proteins in the complex (TP and TPBM).

Author contributions

The manuscript was written through the contributions of all authors. All authors have given approval to the final version of the manuscript.

Funding sources

This work was supported by National Institutes of Health (NIH) grants R56HL123015, R01HL126945, R01EB021926, and R01HL138116, the Ohio State University Office of Undergraduate Research & Creative Inquiry Advanced Summer Research Fellowship, the Ohio State University College of Engineering Honors Research Scholarship and the Pelotonia Fellowship Program. Any opinions, findings, and conclusions expressed in this material are those of the author(s) and do not necessarily reflect those of the Pelotonia Fellowship Program.

5. Conflict of interest disclosure

ISP and AFP are inventors on a pending patent application outlining methods related to protein purification (PCT/US2020/016,267).

CRediT authorship contribution statement

Ivan S. Pires: Conceptualization, Data curation, Formal analysis, Investigation, Methodology, Software, Validation, Visualization, Writing - original draft, Writing - review & editing. **Andre F. Palmer:** Conceptualization, Formal analysis, Funding acquisition, Methodology, Software, Project administration, Resources, Supervision, Validation, Visualization, Writing - original draft, Writing - review & editing.

Declaration of competing interest

The authors declare that they have no known competing financial interests or personal relationships that could have appeared to influence the work reported in this paper.

Acknowledgments

We acknowledge Mani Grevenow (Transfusion Services, Wexner Medical Center, The Ohio State University) for generously donating expired human red blood cell units.

Appendix A. Supplementary data

Supplementary data to this article can be found online at https://doi.org/10.1016/j.memsci.2020.118712.

References

[1] N.E. Labrou, Protein purifi cation: an overview, Methods Mol. Biol. 1129 (2014) 3–10, https://doi.org/10.1007/978-1-62703-977-2_1.
[2] D.J. Pollard, J.M. Woodley, Biocatalysis for pharmaceutical intermediates: the future is now, Trends Biotechnol. 25 (2007) 66–73, https://doi.org/10.1016/j.tibtech.2006.12.005.
[3] D.W. Wood, Non-Chromatographic recombinant protein purification by self-cleaving purification tags, Separ. Sci. Technol. 45 (2010) 2345–2357, https://doi.org/10.1080/01496395.2010.507665.
[4] Y. Fan, J.M. Miozzi, S.D. Stimple, T.C. Han, D.W. Wood, Column-free purification methods for recombinant proteins using self-cleaving aggregating tags, Polymers 10 (2018), https://doi.org/10.3390/polym10050468.
[5] F. Hilbrig, R. Freitag, Protein purification by affinity precipitation, J. Chromatogr. B Anal. Technol. Biomed. Life Sci. 790 (2003) 79–90, https://doi.org/10.1016/S1570-0232(03)00081-3.
[6] M. Iqbal, Y. Tao, S. Xie, Y. Zhu, D. Chen, X. Wang, L. Huang, D. Peng, A. Sattar, M. A.B. Shabbir, H.I. Hussain, S. Ahmed, Z. Yuan, Aqueous two-phase system (ATPS): an overview and advances in its applications, Biol. Proced. Online 18 (2016) 1–18, https://doi.org/10.1186/s12575-016-0048-8.
[7] R. van Reis, A. Zydney, Bioprocess membrane technology, J. Membr. Sci. 297 (2007) 16–50, https://doi.org/10.1016/j.memsci.2007.02.045.
[8] C. Christy, G. Adams, R. Kuriyel, G. Bolton, A. Seilly, High-performance tangential flow filtration: a highly selective membrane separation process, Desalination 144 (2002) 133–136, https://doi.org/10.1016/S0011-9164(02)00301-6.
[9] R. Kaul, B. Mattiasson, Affinity ultrafiltration for protein purification, in: Mol. Interact. Biosep, Springer, US, 1993, pp. 487–498, https://doi.org/10.1007/978-1-4899-1872-7_32.
[10] B. Mattiasson, M. Ramstorp, Ultrafiltration affinity purification. Isolation of concanavalin a from seeds of Canavalia Ensiformis, J. Chromatogr., A 283 (1984) 323–330, https://doi.org/10.1016/S0021-9673(00)96268-X.
[11] T.G.I. Ling, B. Mattiasson, Membrane filtration affinity purification (MFAP) of dehydrogenases using cibacron blue, Biotechnol. Bioeng. 34 (1989) 1321–1325, https://doi.org/10.1002/bit.260341010.
[12] C. Weiner, M. SáRa, G. Dasgupta, U.B. Sleytr, Affinity cross-flow filtration: purification of IgG with a novel protein a affinity matrix prepared from two-dimensional protein crystals, Biotechnol. Bioeng. 44 (1994) 55–65, https://doi.org/10.1002/bit.260440109.
[13] D. Adamski-Medda, Q.T. Nguyen, E. Dellacherie, Biospecific ultrafiltration: a promising purification technique for proteins? J. Membr. Sci. 9 (1981) 337–342, https://doi.org/10.1016/S0376-7388(00)80273-2.
[14] K.J. Hwang, P.Y. Sz, Membrane fouling mechanism and concentration effect in cross-flow microfiltration of BSA/dextran mixtures, Chem. Eng. J. 166 (2011) 669–677, https://doi.org/10.1016/j.cej.2010.11.044.
[15] M.R. Saboktakin, H. Namazi, A.A. Entezami, Determination of the Molecular Weight of Polyacrylamide Fractions by Osmometry, 1993.
[16] M.A. Masuelli, Dextrans in aqueous solution. Experimental review on intrinsic viscosity measurements and temperature effect, J. Polym. Biopolym. Phys. Chem. 1 (2013) 13–21, https://doi.org/10.12691/jpbpc-1-1-3.
[17] E.L. Hess, A. Cobure, THE INTRINSIC VISCOSITY OF MIXED PROTEIN SYSTEMS, INCLUDING STUDIES OF PLASMA AND SERUM*, (n.d).
[18] S. Ilias, K.A. Schimmel, G.E.J.M. Assey, Effect of viscosity on membrane fluxes in cross-flow ultrafiltration, Separ. Sci. Technol. 30 (1995) 1669–1687, https://doi.org/10.1080/01496399508010369.
[19] J. Romero, A.L. Zydney, Chiral separations using ultrafiltration with a stereoselective binding agent, Separ. Sci. Technol. 36 (2001) 1575–1594, https://doi.org/10.1081/SS-100103889.
[20] C.D. Filipe, R. Ghosh, Effects of protein–protein interaction in ultrafiltration based fractionation processes, Biotechnol. Bioeng. 91 (2005) 678–687, https://doi.org/10.1002/bit.20568.
[21] D.M. Kanani, R. Ghosh, C.D.M. Filipe, A novel approach for high-resolution protein-protein separation by ultrafiltration using a dual-facilitating agent, J. Membr. Sci. 243 (2004) 223–228, https://doi.org/10.1016/j.memsci.2004.06.023.
[22] A.F. Palmer, G. Sun, D.R. Harris, Tangential flow filtration of hemoglobin, Biotechnol. Prog. 25 (2009) 189–199, https://doi.org/10.1002/btpr.119.
[23] I.S. Pires, A.F. Palmer, Tangential flow filtration of haptoglobin, Biotechnol. Prog. e3010 (2020), https://doi.org/10.1002/btpr.3010.
[24] C.C. Winterbourn, Oxidative reactions of hemoglobin, Methods Enzymol. 186 (1990) 265–272, https://doi.org/10.1016/0076-6879(90)86118-F.
[25] E. Chiancone, A. Alfsen, C. Ioppolo, P. Vecchini, A.F. Agrò, J. Wyman, E. Antonini, Studies on the reaction of haptoglobin with haemoglobin and haemoglobin chains: I. Stoichiometry and affinity, J. Mol. Biol. 34 (1968) 347–356, https://doi.org/10.1016/0022-2836(68)90258-1.
[26] E. Sada, S. Katoh, K. Sukai, M. Tohma, A. Kondo, Adsorption equilibrium in immuno-affinity chromatography with polyclonal and monoclonal antibodies, Biotechnol. Bioeng. 28 (1986) 1497–1502, https://doi.org/10.1002/bit.260281007.
[27] R. Reverberi, L. Reverberi, Factors affecting the antigen-antibody reaction, Blood Transfus 5 (2007) 227–240, https://doi.org/10.2450/2007.0047-07.
[28] W.C. Olson, T.M. Spitznagel, M.L. Yarmush, Dissociation kinetics of antigen-antibody interactions: studies on a panel of anti-albumin monoclonal antibodies, Mol. Immunol. 26 (1989) 129–136, https://doi.org/10.1016/0161-5890(89)90094-1.
[29] J.N. Herron, E.W. Voss, Analysis of heterogeneous dissociation kinetics in polyclonal populations of rabbit anti-fluorescyl-IgG antibodies, Mol. Immunol. 20 (1983) 1323–1332, https://doi.org/10.1016/0161-5890(83)90163-3.
[30] J.N. Herron, E.W. Voss, An exact procedure for the analysis of heterogeneous kinetics in polyclonal antibody populations, J. Biochem. Biophys. Methods 8 (1983) 189–204, https://doi.org/10.1016/0165-022X(83)90067-2.
[31] F.J. Stevens, Analysis of Protein-Protein Interaction by Simulation of Small-Zone Size-Exclusion Chromatography: Application to an Antibody-Antigen Association1, 1986. https://pubs.acs.org/sharingguidelines. (Accessed 16 January 2020).
[32] F.J. Stevens, Analysis of protein-protein interaction by simulation of small-zone size exclusion chromatography. Stochastic formulation of kinetic rate contributions to observed high-performance liquid chromatography elution characteristics, Biophys. J. 55 (1989) 1155–1167, https://doi.org/10.1016/S0006-3495(89)82912-1.
[33] Q. Li, M. Gordon, C. Cao, K.E. Ugen, D. Morgan, Improvement of a low pH antigen-antibody dissociation procedure for ELISA measurement of circulating anti-Aβ antibodies, BMC Neurosci. 8 (2007) 22, https://doi.org/10.1186/1471-2202-8-22.
[34] N. Zhang, A.F. Palmer, Liposomes surface conjugated with human hemoglobin target delivery to macrophages, Biotechnol. Bioeng. 109 (2012) 823–829, https://doi.org/10.1002/bit.24340.
[35] I.S. Pires, D.A. Belcher, R. Hickey, C. Miller, A.K. Badu-Tawiah, J.H. Baek, P. W. Buehler, A.F. Palmer, Novel manufacturing method for producing apohemoglobin and its biophysical properties, Biotechnol. Bioeng. 117 (2020) 125–145, https://doi.org/10.1002/bit.27193.

[36] F. Polticelli, A. Bocedi, G. Minervini, P. Ascenzi, Human haptoglobin structure and function - a molecular modelling study, FEBS J. 275 (2008) 5648–5656, https://doi.org/10.1111/j.1742-4658.2008.06690.x.
[37] P.K. Hwang, J. Greer, Interaction between hemoglobin subunits in the hemoglobin. Haptoglobin complex, J. Biol. Chem. 255 (1980) 3038–3041. http://www.ncbi.nlm.nih.gov/pubmed/7358726. (Accessed 19 December 2018).
[38] S.R. Wickramasinghe, S.E. Bower, Z. Chen, A. Mukherjee, S.M. Husson, Relating the pore size distribution of ultrafiltration membranes to dextran rejection, J. Membr. Sci. 340 (2009) 1–8, https://doi.org/10.1016/j.memsci.2009.04.056.
[39] K.H. Youm, W.S. Kim, Prediction of intrinsic pore properties of ultrafiltration membrane by solute rejection curves: effects of operating conditions on pore properties, J. Chem. Eng. Jpn. 24 (1991) 1–7, https://doi.org/10.1252/jcej.24.1.
[40] M. Waks, S. Beychok, Induced conformational states in human apohemoglobin on binding of haptoglobin 1-1. Effect of added heme as a probe of frozen structures, Biochemistry 13 (1974) 15–22, https://doi.org/10.1021/bi00698a003.
[41] S.S. Usmani, G. Bedi, J.S. Samuel, S. Singh, S. Kalra, P. Kumar, A.A. Ahuja, M. Sharma, A. Gautam, G.P.S. Raghava, THPdb: database of FDA-approved peptide and protein therapeutics, PloS One 12 (2017), e0181748, https://doi.org/10.1371/journal.pone.0181748.
[42] J.N. Herron, E.W. Voss, Analysis of heterogeneous dissociation kinetics in polyclonal populations of rabbit anti-fluorescyl-IgG antibodies, Mol. Immunol. 20 (1983) 1323–1332, https://doi.org/10.1016/0161-5890(83)90163-3.
[43] R. Ghosh, Novel cascade ultrafiltration configuration for continuous, high-resolution protein-protein fractionation: a simulation study, J. Membr. Sci. 226 (2003) 85–99, https://doi.org/10.1016/j.memsci.2003.08.012.
[44] J. Romero, A.L. Zydney, Staging of affinity ultrafiltration processes for chiral separations, J. Membr. Sci. 209 (2002) 107–119, https://doi.org/10.1016/S0376-7388(02)00283-1.
[45] V.G.J. Rodgers, R.E. Sparks, Reduction of membrane fouling in the ultrafiltration of binary protein mixtures, AIChE J. 37 (1991) 1517–1528, https://doi.org/10.1002/aic.690371009.
[46] A. Jungbauer, N. Walch, Buffer recycling in downstream processing of biologics, Curr. Opin. Chem. Eng. 10 (2015) 1–7, https://doi.org/10.1016/j.coche.2015.06.001.
[47] K. Mohanty, R. Ghosh, Novel tangential-flow countercurrent cascade ultrafiltration configuration for continuous purification of humanized monoclonal antibody, J. Membr. Sci. 307 (2008) 117–125, https://doi.org/10.1016/j.memsci.2007.09.010.
[48] M. Mayani, K. Mohanty, C. Filipe, R. Ghosh, Continuous fractionation of plasma proteins HSA and HIgG using cascade ultrafiltration systems, Separ. Purif. Technol. 70 (2009) 231–241, https://doi.org/10.1016/j.seppur.2009.10.002.
[49] M. Mayani, C.D.M. Filipe, R. Ghosh, Cascade ultrafiltration systems-Integrated processes for purification and concentration of lysozyme, J. Membr. Sci. 347 (2010) 150–158, https://doi.org/10.1016/j.memsci.2009.10.016.
[50] R. van Reis, E.M. Goodrich, C.L. Yson, L.N. Frautschy, S. Dzengeleski, H. Lutz, Linear scale ultrafiltration, Biotechnol. Bioeng. 55 (1997) 737–746, https://doi.org/10.1002/(SICI)1097-0290(19970905)55:5<737::AID-BIT4>3.0.CO;2-C.